Halogen cycling and precious metal enrichment in sub-volcanic magmatic systems

DOI:
10.1016/j.epsl.2019.115769

Document Version
Accepted author manuscript

Halogen cycling and precious metal enrichment in sub-volcanic magmatic systems: insights from the Rum layered intrusion, Scotland

Amy P. Parker[1], Patricia L. Clay[1], Ray Burgess[1], Hélène Balcone-Boissard[2], Pierre Bürckel[3] and Brian O'Driscoll[1]

[1]School of Earth and Environmental Sciences, University of Manchester, Manchester, M13 9PL, UK.
[2]Sorbonne Universités, UPMC Université Paris 06, CNRS, Institut des Sciences de la Terre de Paris (ISTeP), 4 place Jussieu, 75005 Paris, France.
[3]Institut de Physique du Globe de Paris, Sorbonne Paris Cité, Univ. Paris Diderot, CNRS, F-75005 Paris, (France)

Amy.parker@manchester.ac.uk

Highlights:

- NI-NGMS is a sensitive method for tracing halogen provenance and evolution in magmatic systems
- Rum halogens exhibit a broad scatter between mantle- and sedimentary-like halogens
- PGE-rich chromitites preserve evidence of a high-I (sedimentary) component

Halogen cycling and precious metal enrichment in sub-volcanic magmatic systems: insights from the Rum layered intrusion, Scotland

Amy P. Parker[1], Patricia L. Clay[1], Ray Burgess[1], Hélène Balcone-Boissard[2], Pierre Bürckel[3] and Brian O'Driscoll[1]

[1]School of Earth and Environmental Sciences, University of Manchester, Manchester, M13 9PL, UK.

[2]Sorbonne Universités, UPMC Université Paris 06, CNRS, Institut des Sciences de la Terre de Paris (ISTeP), 4 place Jussieu, 75005 Paris, France.

[3]Institut de Physique du Globe de Paris, Sorbonne Paris Cité, Univ. Paris Diderot, CNRS, F-75005 Paris, (France)

Amy.parker@manchester.ac.uk

Keywords: Halogens; noble gas isotopes; Rum Layered Suite; platinum-group elements; crustal contamination

Abstract

The cycling of the halogens in sub-volcanic systems may play an important role in magmatic ore deposit formation and the emission of climate-altering gases via volcanic outgassing. However, the mobile and reactive nature of the halogens, as well as their typically low abundances in most intrusive igneous rocks, means that their behaviour in shallow crustal level magmatic systems is difficult to constrain. We present data from the ~60 Ma Rum Layered Suite, NW Scotland, utilising the neutron irradiation-noble gas mass spectrometry (NI-NGMS) technique, to provide insight into the provenance and behaviour of Cl, Br and I in magma chamber processes and precious metal enrichment. As a well-characterised and superbly exposed example of an open system sub-volcanic magmatic body, the Rum intrusion is an ideal locality to investigate halogen behaviour in this context. Our data reveal concentrations of <1 ppm to 124 ppm for Cl, <7 ppb to 484 ppb for Br and ~1 ppb to 363 ppb

for I in the Rum rocks. Halogen ratios span a range of 2.3 x 10^{-4} to 1.5 x 10^{-2} for Br/Cl and 4.0 x 10^{-5} to 7.4 x 10^{-2} for I/Cl, defining an array from MORB-like to sedimentary-like halogen ratios. Chlorine and Br behave sympathetically in all lithologies, and in the rocks considered to be primary magmatic differentiates (i.e., peridotites, troctolites and gabbros), the variation in abundances is likely controlled by accessory quantities of primary hydrous magmatic phases crystallising from the mush interstitial liquid. Iodine behaviour is decoupled from that of Br and Cl, and combined with noble gas isotope data, suggests variable but pervasive contamination by a sedimentary source or sources during crystallisation of the Rum intrusion. In PGE-rich chromitites, high I/Cl ratios relative to their putative picritic parental melts point to the involvement of a crustal I source and hydrous fluids during chromitite formation. Our combined halogen and noble gas isotope datasets therefore reveal a record of high temperature processes associated with magmatic-crustal interactions and precious metal mineralisation, and provide new insights into volatile evolution during solidification of the Rum intrusion. A key implication of this work is that magma-crust interactions in mafic magmatic systems may lead to I concentration (i.e., from 12% to up to two orders of magnitude greater than MORB, in the Rum intrusion), before potential outgassing to the atmosphere.

1. Introduction

The heavy halogen group elements, chlorine, bromine, and iodine, are a suite of highly incompatible, reactive, and fluid mobile elements that are common constituents of high-temperature volcanic emissions (e.g., Aiuppa *et al.* 2009; Allard *et al.* 2016). Despite their relatively low abundances, halogen concentrations in silicate magmas have great significance in terms of releasing harmful and climate-altering volcanic gases to the atmosphere (von Glasow *et al.* 2009), as well as affecting magma viscosity and explosivity during volcanic eruptions (e.g., Pyle and Mather, 2009) and playing a role in rock alteration by hydrothermal fluids (Reed 1997). The halogens, especially Cl, also play an influential role in the transportation and redistribution of metals during the formation of magmatic ore

deposits (Halter and Webster 2004; Aiuppa *et al.* 2009). For example, the addition of chloride salts to aqueous fluids produces negatively-charged ligands that complex with positive metal ions, effectively increasing metal solubilities (cf. Lecumberri-Sanchez and Bodnar 2018).

Layered mafic-ultramafic intrusions are considered to represent the solidified remnants of basaltic magma chambers (O'Driscoll and VanTongeren 2017), and host the majority of the world's exploited platinum-group element (PGE) deposits (Mungall and Naldrett 2008). The crystallisation of layered intrusions is the result of chemical and physical processes including magmatic differentiation and magma-crust interaction. These systems therefore represent ideal natural laboratories for evaluating the geochemical evolution of magma in sub-volcanic reservoirs. Layered intrusion-hosted PGE are principally associated with base-metal sulfides that concentrate in stratiform 'reefs'; however, there is continued debate over the mechanisms by which the PGE-enrichment occurs. Orthomagmatic models focus on immiscible sulfide liquid as a scavenging agent for the PGE. Here, the driver for sulfide liquid segregation is magma mixing or assimilation of crustal materials or the magma chamber walls/floor-rock (Mungall and Naldrett 2008). Alternatively, metasomatic processes involving the percolation of halogen-rich fluid through the footwall have been invoked (e.g., for the J-M Reef of the Stillwater Complex, USA; Boudreau *et al.* 1986; Hanley *et al.* 2008). However, the behaviour of Cl and especially Br and I during the formation of PGE-deposits in layered intrusions remains poorly constrained. This is due in part to the highly mobile and reactive nature of the halogens, as well as their low abundance in typical layered intrusion lithologies, meaning that direct evidence of volatile activity is difficult to detect.

In order to elucidate the role of the halogens in PGE-reef formation, as well as evaluate the processing of the halogens in sub-volcanic basaltic magmatic systems more generally, we have carried out a detailed study of halogen abundances in the Rum Layered Suite (RLS), NW Scotland. The heavy halogens range from moderately to highly incompatible and therefore their distribution should be influenced by first order magmatic processes, such as partial melting, fractional crystallisation and degassing (Aiuppa *et al.*

2009). As fluid mobile elements, they should also be strongly affected by the presence of aqueous fluids. The Rum intrusion is an ideal locality to carry out this work as it has undergone relatively little post-emplacement alteration and is otherwise well-characterised in terms of its petrology and geochemistry (e.g., Brown 1956; Bédard *et al.* 1988; Greenwood *et al.* 1992; Emeleus *et al*., 1996; O'Driscoll *et al.* 2009; 2010). We employ the neutron-irradiation noble gas mass spectrometry (NI-NGMS) technique to measure the heavy halogen (Cl, Br and I) abundances of PGE-enriched chromitite seams, picrite dykes (representative of the Rum parental melts), various magmatic differentiates (i.e., cumulates such as peridotites, gabbros), pegmatoids (representing late-stage volatile-rich magmas) and their mineral separates (e.g., olivine, amphibole, sulfides). The Rum intrusion was emplaced into metamorphic and sedimentary rocks of variable age and composition, and an ancillary aim of this study is to examine whether or not the halogens and noble gas isotope ratios can be used to trace magma-crust interactions.

2. Geological setting and sample details

The Rum Layered Suite (RLS; Fig. S1) formed at 60.53 ±0.08 Myr (Hamilton *et al.* 1998) during opening of the North Atlantic and magmatism associated with the present-day Iceland mantle anomaly, as part of the British Palaeogene Igneous Province (BPIP). The RLS intruded into a suite of rocks comprising Archean basement (Lewisian Complex) gneisses and Neoproterozoic (Torridonian Supergoup) sandstones, as well as a succession of Mesozoic sediments (Emeleus *et al.* 1996). The Torridonian rocks are largely unmetamorphosed and comprise arkosic sandstones and shales. The Mesozoic sedimentary rocks include a condensed sequence of Triassic breccias and sandstones (~80 m thick; Emeleus *et al.* 1996), and fault-bound slivers of Lower Jurassic limestone, sandstone and mudstone which are thermally metamorphosed by the RLS (Fig. S1c).

The RLS exhibits evidence for open system magma chamber behaviour and is sub-divided into three portions; the Eastern, Western and Central Layered Intrusions (Fig. S1b). The Eastern Layered Intrusion (ELI; Fig. S1d) comprises 16 individual cyclic units, each

thought to represent a new influx of basaltic and/or picritic composition magma, with a peridotite base and troctolite (±olivine gabbro and anorthosite) top (Brown 1956; Emeleus *et al.* 1996). Platinum-group element-enriched Cr-spinel seams (chromitite), typically 2-4 mm thick, occur at the boundaries between some units (e.g. 7-8 and 11-12; e.g. O'Driscoll *et al.* 2009). Anhedral accessory base-metal sulfide grains (<0.1 mm) occur within these chromitite seams, and are the primary hosts for the PGE mineralisation (O'Driscoll *et al.* 2009). The chromitite seams were originally interpreted as the product of crystal settling onto the plagioclase-rich magma chamber floor (e.g., Brown 1956); however, recent investigations have advocated an *in situ* crystallisation model for the chromitites (O'Driscoll *et al.* 2010).

Thirty samples were selected for halogen abundance measurements, including bulk rock and mineral separates, from various lithologies throughout the intrusion (see Table S1 for further details). An important goal of this study is to investigate the halogen geochemistry of the PGE-reefs, so detailed transects across the Unit 7-8 and 11-12 chromitite seams were carried out including footwall and hanging wall lithologies. The mineralogy and field relationships of these rocks have been previously described (e.g., O'Driscoll *et al.* 2009, 2010). Magmatic differentiates from parts of the Rum intrusion devoid of chromitite seams were also sampled (e.g., Unit 9). A selection of picrite dykes, considered proxies for the parental magmas that formed the Rum magma chamber, was included. Olivine separates were analysed from two picrite samples (RM_16_010 and RM_16_012). Sulfide-bearing troctolites (RM17) of the contact zone formed due to contamination of magma by S-bearing sedimentary rocks (Hulbert *et al.* 1992), so were analysed to investigate a potential country rock halogen signature. Similarly, samples from sulfide-bearing peridotite in a satellite plug (outside the RLS; RM_16_017; Fig. S1) were analysed. Finally, a suite of late-stage pegmatoids were analysed. Some of the pegmatoids occur at the tops of the macro-rhythmic units (Units 10, 11) and are considered to represent compaction-driven expulsion of interstitial melt from the underlying crystal mush (Emeleus *et al.* 1996). Another pegmatoid (RM_16_021) comes from the Central Intrusion, part of a suite that was dated by Hamilton *et*

al. (1998) as the youngest magmatism associated with the RLS. A variety of country rocks, including Jurassic mudrocks, Triassic sediments and Torridonian Supergroup sandstones, were also analysed.

3. Analytical techniques

3.1 Electron microscopy

In order to gain a qualitative overview of halogen distribution in key samples (e.g., the PGE-rich chromitite seams), X-ray mapping was carried out using the Cameca SX-100 electron microprobe in Manchester. Chlorine maps were conducted at an acceleration voltage of 15 kV and 200 nA beam current.

3.2 Halogen abundances and noble gas isotopes by neutron irradiation

A detailed description of the NI-NGMS technique and our sample preparation methodology is provided in the supplement (S1.1) and in Ruzié-Hamilton *et al.* (2016). NI-NGMS utilises the neutron conversion of Cl, Br and I into their respective noble gas proxy isotopes [(n, γ, β) reaction; producing ^{38}Ar from Cl, ^{80,82}Kr from Br, and ^{128}Xe from I]. The method enables measurement of the heavy halogens and the natural noble gases simultaneously. Measurements of the halogens were conducted on the Thermo Scientific Argus VI™ noble gas mass spectrometer at the University of Manchester. Data were corrected for blanks (conducted after every 3-4 measurements) and mass discrimination (monitored daily using air calibrations). Blank contributions were typically <<1 % (but up to 3%) for ^{38}Ar, and <<0.1 % for ^{80,82}Kr and ^{128}Xe. Data were also corrected for decay of ^{37}Ar and ^{39}Ar, air contributions, and neutron-induced reactions producing ^{40}Ar, ^{39}Ar, ^{38}Ar and ^{36}Ar, monitored by the K and Ca salts placed in the irradiation (Table S2). Individual replicate data is provided together with specific sample details in Table S2 of the supplement. Between two and five replicate analyses have been averaged for each sample. Halogen elemental ratios are reported as weight ratios and uncertainties quoted to 1 standard error of the mean of the replicate averages provide a measure of sample heterogeneity.

172

173 *3.3 Halogen abundances after pyrohydrolysis extraction*

174 The halogen abundances of a selection of Rum sedimentary rocks were measured using the
175 pyrohydrolysis technique, a detailed description of which is given in the supplement (S1.2)
176 and in Balcone-Boissard *et al.* (2009) and Schnetger and Muramatsu (1996). Hydrolysis
177 solutions were analysed by ion chromatography for F and Cl and inductively coupled
178 plasma-mass spectrometry (ICP-MS) for Br and I. This method was employed for the
179 sedimentary samples rather than NI-NGMS due to the technical difficulties of producing
180 high-precision measurements in materials containing abundant organic materials and
181 carbonates (e.g., Mesozoic mudstones).

182

183 **4. Results**

184 *4.1 Mineral-scale observations*

185 The volume proportion of interstitial minerals (representing crystallised interstitial melt) is
186 variable for the peridotites, troctolites and gabbros. However, hydrous minerals (e.g., biotite,
187 serpentine and amphibole) are a ubiquitous accessory phase in all of these rocks, occurring
188 at the boundaries or triple grain junctions between primocrysts and interstitial phases (Fig.
189 S2a). No apatite is observed. No textural evidence for degassing or fluid escape is observed
190 in any of these rocks. The picrite dykes are mainly olivine-phyric, with a fine-grained
191 groundmass comprising intergrown plagioclase and clinopyroxene, but one sample
192 (RM_16_011) is aphyric and exhibits a spinifex-type ‘quench’ texture suggesting rapid
193 solidification (Fig. 1a). The pegmatoids contain minor amounts of hydrous phases (biotite
194 and amphibole) and apatite, except for pegmatoid (RM_16_021), which has abundant
195 amphibole and biotite, as well as apatite and zircon (Fig. 1b).

196 Chromitite seams are always associated with a greater proportion (1-2 vol.%) of
197 hydrous minerals than their host rocks. Biotite and amphibole occur as anhedral crystals in
198 interstitial areas to Cr-spinel crystals, as spherical inclusions in Cr-spinel and adjacent
199 olivine crystals (Fig. S2b,c), and in thin (<1 mm) veins that cross-cut the primary minerals

(Fig. S2d). The Cl X-ray maps of the Unit 7-8 boundary chromitite also reveal the presence of rare apatite grains (<50 µm in size), commonly associated with biotite (Fig. 1c,d). The apatite has moderate to low Cl contents of <0.4 wt.%. Biotite grains (<1 mm) also appear to have relatively low Cl contents (<0.1 wt.%). Element mapping of Cl highlights extensive and pervasive alteration veining along olivine grain boundaries and intra-crystal fractures.

4.2 Heavy halogen abundances and ratios for the Rum intrusion and country rocks

The halogen abundance and noble gas isotope data for the Rum samples are presented in Table 1 and in Figures 2-4. Chlorine, Br and I concentrations range from 1 ppm to 124 ppm, 7 to 484 ppb and <1 to 363 ppb, respectively, in bulk samples and mineral separates. In general, Br and Cl abundances are positively correlated (Fig. 2a); however, I and Cl are not correlated (Fig. 2b). Intra-sample variation was not significant in most cases (e.g., within ~ 15%) and likely reflects natural sample variability. This is particularly true for some bulk samples, for instance the B2 Peridotite, where concentrations are low (i.e., <10 ppm Cl) and therefore the variation over repeat analyses (2-10 ppm Cl over 5 analyses ~62% variation) is higher.

Picrites. Picrite samples (n=3) have Cl concentrations of 23-75 ppm, 89-229 ppb Br and 4-19 ppb I. Picrite olivine separates (n=2) display systematically lower halogen contents (Cl = 6-13 ppm; Br = 43-48 ppb; I = 0.5-2 ppb). The picrites define a trend to high Cl and low ^{40}Ar (Fig. 3a), distinct from most other RLS rocks.

Rum intrusion magmatic differentiates. Peridotites (n=3) overlying the chromitite seams have halogen contents of 3-16 ppm Cl, 2-78 ppb Br and 1-4 ppb I. Troctolites and olivine gabbros (n=3) range from ~1-83 ppm Cl, 14-84 ppb Br and 3-60 ppb I. In the Unit 1 troctolite (RM17), for which a sulfide separate and bulk rock were analysed, the sulfide shows higher I concentrations compared to bulk rock (24 ppb to 6 ppb, respectively) whilst Cl is similar (~4 ppm). Chromitites (n=4) have halogen contents of 2-3 ppm Cl, 9-35 ppb Br and 10-102 ppb I. The Unit 7-8 chromitite has high I (75 ppb) compared to Br (29 ppb) and Cl (2 ppm; Fig. 2a,b). In contrast, the Unit 11-12 chromitite seam has lower Br (10 ppb) and I

(17 ppb). Chromitites have low Cl/^{36}Ar ratios and define a trend towards high ^{40}Ar and low Cl (Fig. 3a, b). The anorthosites (n=3), some of which are closely associated with the chromitite seams (n = 4), display higher concentrations of Cl (e.g., 11 ppm in the Unit 7 anorthosite) compared to the chromitite seams, but variable I (29 ppb Unit 7 anorthosite, 50 ppb Unit 11 anorthosite).

Satellite intrusion rocks. Peridotite plugs (n=2) have halogen abundances of 16 and 99 ppm Cl, 67 and 394 ppb Br and 21 and 50 ppb I.

Pegmatoids. Pegmatoids (n=4) yield highly variable halogen abundances. Chlorine contents range from 2-53 ppm, Br ranges from 7-144 ppb and I from 2-363 ppb. Associated mineral separates, including biotite (n=1) and amphibole (n=3) also show variation. Amphiboles have halogen contents of 1-39 pm Cl, 7-20 ppb Br and 2-104 ppb I. Biotite (124 ppm Cl, 29 ppb Br and 200 ppb I) is also Cl- and I-rich.

4.3 Halogens in the Rum intrusion country rocks

Halogens, including F, were analysed for a selection (n=7) of RLS country rocks including Mesozoic sandstones and limestones, as well as Torridonian sandstones (Table S3). The sedimentary rocks all exhibit concentrations of the heavy halogens that are at the upper end of the array defined by the RLS rocks (Fig. 2). One calcareous sandstone of Mesozoic (Triassic) age has a high I/Cl ratio of 0.51 resulting from an I concentration of 3227 ppb and a relatively low Cl concentration (6 ppm).

4.4 Noble gas isotope systematics

Noble gas ratios, such as ^{130}Xe/^{36}Ar and ^{84}Kr/^{36}Ar, have well-defined compositions for air, MORB, seawater and sedimentary rocks (Fig. 4). The RLS data exhibit a degree of scatter, with no consistent variation, and the sample set overall yields ranges between ~ 17-125 x 10^{-3} for ^{84}Kr/^{36}Ar and 0.2-4.8 x 10^{-3} for ^{130}Xe/^{36}Ar. Hence, the data range from MORB-like (^{84}Kr/^{36}Ar = 0.05, ^{130}Xe/^{36}Ar ~1 x 10^{-3}, Moreira *et al.*, 1998; Holland and Ballentine, 2006) to the field for submarine sediments (^{84}Kr/^{36}Ar = 0.1 - 0.2 and ^{130}Xe/^{36}Ar = 2-3 x 10^{-3}; Matsuda

and Nagano, 1986; Staudacher and Allègre, 1988), with some clustering of the data close to the seawater value $^{84}Kr/^{36}Ar$ = 0.04, $^{130}Xe/^{36}Ar$ = 5 x 10^{-4} (Holland and Ballentine, 2006; Kendrick *et al.*, 2013).

5. Discussion

Halogen ratios (Br/Cl and I/Cl) are useful for discriminating between specific reservoirs (e.g., MORB, sediments, etc.; Tables 1, S2; Fig. 2c). The RLS displays significant variations in halogen concentrations and ratios throughout the intrusion, with a broad general trend from mantle-like values (2.86 ±0.6 and 60 ±30 x 10^{-6} wt. Br/Cl and I/Cl; Kendrick *et al.* 2012; 2013; 2014) in the picrites towards fields for sedimentary rock compositions (Fig. 2c). The ELI exhibits elevated I/Cl compared to the picrite samples and MORB and OIB values in general. This is especially true of certain pegmatoids and chromitite horizons, where I concentrations are significantly higher and decoupled from Cl and Br (Fig. 2b). In the following sections, we discuss these trends in the context of primary magmatic (i.e., magma differentiation-related) processes, mineralogical controls on the halogens and secondary processes (including crustal contamination and late-stage alteration).

5.1 The Rum parental magmas and primary magmatic processes

Parental melt characteristics. The RLS and associated intrusions, including the picrite dykes and satellite plugs (Emeleus et al. 1996; Upton *et al.* 2002; Meyer *et al.* 2009), are the result of Palaeogene volcanism associated with opening of the North Atlantic Ocean and proto-Iceland plume activity. Picrites reveal Br/Cl and I/Cl ratios that are similar to established mantle values (e.g., Kendrick *et al.* 2012, 2013, 2014), consistent with previous suggestions for the composition of the Rum mantle source region (O'Driscoll *et al.* 2009). Br/Cl and most of the I/Cl sample ratios lie close (within an order of magnitude) to the MORB trend (Fig. 2a,b), further supporting a primary origin for the picrite halogens. The picrite samples exhibit amongst the highest Cl concentrations in our Rum dataset. Given that these rocks represent the primitive magmas that formed the Rum intrusion, we suggest that Cl has been

subsequently lost during the magma chamber processes responsible for crystallisation of the cumulate lithologies (peridotites, troctolites and gabbros). Conversely, the picrites have <11 ppb iodine, a factor of 2-10 lower than I in many of the Rum intrusion rocks.

Magmatic differentiation. Bromine and Cl abundances correlate well throughout the Rum intrusion rocks (Fig. 2a), from typically low Br and Cl in the chromitites and anorthosites, to higher Br and Cl in the picrites and peridotites. Troctolite and gabbro samples vary along this spectrum. Iodine and Cl, however are not well-correlated and show no trend with compositional group (except for the picrites, which lie close to the MORB line; Fig. 2b). This suggests that the process(es) or phase(s) (minerals, inclusion, etc.) controlling Br and Cl distribution in these rocks is the same, whilst I behaviour is different. Here, we evaluate the potential for fractional crystallisation to explain the halogen variations observed. The halogens are highly incompatible elements ($D_{halogen}^{mineral/melt}$<<1) and thus should behave similarly during progressive crystallisation of magma. Major element fractional crystallisation indices (e.g., Ni and Al_2O_3 versus MgO content; Fig. S3a,b) correlate well with mineral abundances in the cumulates. However, halogen abundances and ratios show no correlation with MgO content (Fig. S4a-c). Calculations based on estimated bulk partition coefficients for Cl and Br show no significant fractionation of these elements from one another during crystallisation of the parental melt (Table S4, Fig. S5), in agreement with the Rum data (Fig. 2a). Therefore, halogen distributions in the cumulates are not explained by simple fractional crystallisation processes, in line with previous studies on basaltic glass (e.g., Schilling *et al.,* 1980, Kendrick *et al.,* 2013), which have shown that halogens are not fractionated by melting and crystallisation processes.

Shallow-level magmatic degassing and fluid-melt partitioning. Rum cumulates are Cl-deficient compared to the picrites considered to be their parental magma(s). Here we examine if shallow magmatic degassing processes can explain these differences. Halogen degassing into the vapour phase is expected only at pressures <1 MPa (Edmonds *et al.,* 2009), but partitioning of halogens into aqueous fluid is considered. Chlorine partitions

preferably into the fluid phase over the melt ($D_{Cl}^{fluid/melt}$ >>1) across most of the range of P-T conditions relevant to shallow-crustal magmatic systems. Limited data for Br and I partitioning between fluid and melt exist for felsic magmas (e.g., albitic melt) and indicate that $D_{Cl}^{fluid/melt}$ ~8, $D_{Br}^{fluid/melt}$ ~18 and $D_{I}^{fluid/melt}$ ~ 104 (Bureau *et al.,* 2000). Therefore, in the presence of aqueous fluid, the halogens should degas in the order I>>Br>Cl, meaning even minor degassing could influence the halogen budget of the RLS.

Experimental constraints (Webster *et al.* 1999; Alletti *et al.,* 2009) suggest that the maximum Cl capacity of a melt analogous to the Rum parental magma is ~2.15 wt.% (Fig. S6a), whilst melt inclusion data indicate that mafic silicate melts contain a maximum of 0.5-1.0 wt.% Cl (Webster et al., 1999). These values exceed the ~75 ppm measured in picrite RM_16_011, suggesting either an initially Cl-poor melt or degassing of Cl into an aqueous fluid (e.g., a first boiling process driven by H_2O exsolution). At ~2 km depth (4.9 x 10^7 Pa), a reasonable depth of emplacement for the Rum magma chamber (Holness 1999), ($D_{Cl}^{fluid/melt}$= 9.1 (Fig. S6b; Alletti et al., 2009), suggesting that early aqueous fluids exsolved from the RLS magmas could have removed significant Cl (Fig. S6c). Despite experimental and melt inclusion constraints suggesting the potential for high Cl concentrations, petrographic and geochemical evidence for the aqueous fluid required to extract the halogens is absent from the Rum cumulates. For instance, only small amounts (<1 vol. %; see above) of hydrous magmatic minerals (e.g., biotite and apatite) are present. Furthermore, there is no evidence of fluid inclusions and the loss on ignition (LOI) values for the cumulates are low (typically <0.5 wt.% and up to 1.70 wt. %; O'Driscoll *et a*l. 2009). We therefore suggest that the Rum parental melt was either Cl-poor or very efficiently degassed during pre-crystallisation first boiling, due to the high ($D_{Cl}^{fluid/melt}$, along with the H_2O that drove degassing, a process for which no field or petrographic evidence now remains.

Mineralogical controls on halogen distributions. Previous work on the trace element geochemistry, as well as the radiogenic and stable isotope systematics of the RLS have shown that low temperature alteration and/or hydrothermal processes did not play a major

role in during the evolution of the Rum intrusion (e.g., Palacz 1985; Greenwood *et al.* 1992; Meyer *et al.* 2009; O'Driscoll *et al.* 2009). The mineralogy and textures of RLS rocks (particularly the cumulates) support this suggestion; alteration is generally minor and spatially confined (e.g., localised alteration veins in chromitites; **Fig. 1b**), with no evidence for widespread low-temperature modification or recrystallisation.

The cumulate rocks are mixtures between primocrysts and interstitial melt. In line with other work on these rocks (Emeleus *et al.* 1996), we interpret the accessory hydrous phases present as reflecting volatile enrichment in the residual liquid, during progressive crystallisation of the crystal mush. By contrast, the chromitites contain microstructural evidence for volatile mobility, including greater amounts of interstitial biotite and apatite, and secondary biotite-amphibole-bearing veins. In order to determine if the hydrous phases might control the bulk rock halogen abundances, contributions from these phases can be compared to bulk rock halogen abundances. The modal proportions of apatite, biotite and amphibole required to account for bulk rock Cl, are calculated using halogen concentrations (**Fig. S7** and **Table S5a**) in these phases, estimated from the amphibole and biotite separates analysed from the Rum pegmatoids (these rocks are not directly petrogenetically related, but aid a first order approximation). Apatite was approximated using the median halogen composition of OH apatite (Kusebach *et al*., 2015). Apatite can account for the lowest bulk Cl abundances (<0.5 vol.%), but not Cl in the highest abundance samples, which would require ~10 vol.% apatite. Apatite can account for the highest Br and I abundances (<3.9 vol.%); however, a lack of correlation between bulk rock P_2O_5 and any of the heavy halogens suggests that apatite alone does not control halogen contents (**Fig. S7d**). Biotite and amphibole can account for the lowest I abundances only (<0.6-1.1 vol.%). Therefore, whilst the full range of Br and I abundances in the Rum rocks can be best accounted for by apatite, biotite, which is ubiquitously present, is a more realistic carrier for halogens in all but the highest concentration samples (the latter do contain apatite). A caveat is that Br and I whole rock abundances show no correlation in these rocks (which would be expected if they were hosted by the same phase) yet Cl and Br are strongly correlated. Thus, we conclude

365 that the heavy halogen budgets of the cumulates are controlled in general by hydrous
366 accessory phases related to the final stages of crystallisation of the interstitial liquid, and the
367 precise nature of the control on the variations between lithologies is likely a function of
368 contributions from mixtures of these phases in each whole rock sample.
369
370 *5.2 Magma-crust interactions and the high I component in the RLS*
371 *The Rum I source.* Chlorine and Br are present in MORB-relative abundances in the RLS
372 rocks. Iodine, however, is decoupled from Cl and Br in its abundance and ratio patterns and
373 requires an alternative explanation. We therefore consider the role of crustal contamination
374 to explain the high I seen in some lithologies (e.g., Déruelle *et al.* 1992; Muramatsu and
375 Wedepohl 1998). Studies based on different radiogenic isotopic techniques (e.g., Sr, Nd, Os)
376 have demonstrated that the RLS rocks preserve evidence for crustal contamination (Palacz
377 1985; Meyer *et al.* 2009; O'Driscoll et al. 2009). Palacz (1985) estimated contamination of
378 the Rum parental magma by up to 7% Lewisian Complex gneiss to account for Sr isotope
379 signatures in the RLS cumulates. Similarly, O'Driscoll *et al.* (2009) suggested 5-8%
380 contamination of a suite of Rum rocks by Lewisian gneiss on the basis of Os isotope data.
381 Upton *et al.* (2002) calculated ≤4% crustal contamination of a suite of picrite dykes, including
382 the M9 picrite from this study, on the basis of Sr, Nd and Pb isotopes. Here, we consider the
383 role that contamination by Torridonian Supergroup and Mesozoic sedimentary country rocks
384 may have had. Whilst we have no halogen data for the basement Lewisian gneisses, it is
385 unlikely that they contributed significant amounts of heavy halogens, particularly I, to RLS
386 magmas (because of pre-intrusion metamorphism and their initially low abundances – they
387 mainly have igneous protoliths).
388 Due to its biophilic behaviour, I is enriched in organic sediments (e.g., marine shales)
389 and is a sensitive indicator of contamination by sediments (Li and Schoomaker 2003;
390 Muramatsu and Wedepohl 1998; Kendrick *et al.* 2017). The I concentrations of the
391 sediments that may have yielded the fluid contaminant range from 11-183 ppb (n=3,
392 Jurassic mudstones and calcareous sediments), 33-3227 ppb (n=2, Triassic sandstone and

393 calcareous sediment) and 47-122 ppb I (n=2, Torridonian sandstones). For comparison, the
394 bulk continental crust has an estimated I concentration of 700 ppb (Rudnick and Gao, 2003).
395 Assuming solid assimilation of country rock, different degrees of contamination would be
396 required to account for the variation in I enrichment relative to the picrites (maximum I = 11
397 ppb). Iodine enrichment is not lithology dependant; high-I (>45 ppb) samples include
398 peridotite, troctolite, anorthosite and chromitite (**Table 1**). Using average I concentrations for
399 each of the country rock reservoirs, assimilation of 0.1-6.2% of the Triassic rocks best
400 accounts for the elevated I abundances seen in the RLS rocks in terms of consistency with
401 previous studies (Tables S3; S5b; Palacz 1985; Meyer *et al.* 2009; O'Driscoll et al. 2009).
402 Torridonian sandstones and Jurassic sediments require greater degrees of assimilation
403 (>10% and 15%, respectively) to account for even the lowest levels of I enrichment in the
404 RLS rocks. The Rum intrusion was emplaced close to the unconformity between the
405 Lewisian gneisses and the Torridonian rocks, and clearly interacted with Mesozoic rocks too,
406 so it is likely that mixtures of these different reservoirs interacted with the Rum parental
407 melts (see below).

408 Direct country rock assimilation can explain the ubiquitous enrichment of I in the Rum
409 samples, relative to MORB. The picrites show the lowest I concentrations, lying closest to
410 the MORB reference line (Fig. 2b), and supporting their interpretation as proxies for the Rum
411 parental melts. However, assimilation of solid country rock would not obviously fractionate I
412 from Br and Cl (i.e., addition of halogens would be congruent) in the manner shown by the
413 data (Fig. 2b), so it is useful to further consider the nature of the contaminant that introduced
414 I into the RLS magmas. As noted above, the cumulate lithologies do not preserve any field
415 or petrographic evidence for significant fluid flow. However, it is possible that the pervasive I
416 enrichment in the RLS rocks reflects addition to the parental melts of fluid generated by
417 dehydration of country rocks such as the Triassic sediments, prior to crystallisation of the
418 cumulates. Based on what little is known about I partitioning (e.g., in felsic systems a high
419 fluid-melt partition coefficient of D ~ 104; Bureau et al., 2000), even small amounts of fluid
420 extracted during devolatilisation of sediments would likely contain enough I to account for the

relative enrichment over the picrites, whilst accounting for the low LOI and low abundances of hydrous phases in the RLS rocks. It is worth noting that the Jurassic country rocks occur in fault-bound blocks in close proximity to the intrusion and may have undergone devolatilisation-related I loss, relative to Cl (11 ppb versus 34 ppm, respectively; Fig. 2c), based on comparisons with a global marine shale average (Li and Schoonmaker 2003).

Evidence of crustal contamination from noble gas isotope signatures. The RLS noble gas isotope data lend support to crustal contamination sourcing some of the halogens. Many samples (including chromitites, cumulates and pegmatoids) trend towards and into a field in $^{130}Xe/^{36}Ar$ versus $^{84}Kr/^{36}Ar$ space defined by oceanic sediments (Fig. 4). Elevated $^{130}Xe/^{36}Ar$ ratios are often measured in marine shales due to their high organic content (e.g., Ozima and Podosek 2002); therefore, the enriched $^{130}Xe/^{36}Ar$ and $^{84}Kr/^{36}Ar$ ratios may suggest assimilation of Mesozoic sedimentary rocks into the Rum parental magmas. The Ar isotope data are also useful here. We calculated age-corrected $^{40}Ar/^{36}Ar$ ratios, based on the anticipated ingrowth of radiogenic Ar (over 60.53 ±0.08 Ma; Hamilton *et al.* 1998) for the RLS and measured K concentrations (Table S2). The K-contents of the RLS samples are generally low (~40-3000 ppm; with the exception of some pegmatoid samples), and therefore ingrowth cannot have led to the $^{40}Ar/^{36}Ar$ ratios observed, over ~60 Ma. A wide range (330-9300) in $^{40}Ar/^{36}Ar$ ratios is observed (Table S2; Fig. 3a), and the age-correction for ^{40}Ar results in only a small change to the $^{40}Ar/^{36}Ar$ ratio, on the order of 0.1-1%. The lowest, air-like ratios ($^{40}Ar/^{36}Ar$ air = 298.6; Lee *et al.*, 2006), occur in the ELI pegmatoids and satellite plug and the highest ratios are exhibited by some cumulates (Fig. 3a). Mineral separates, such as amphibole, clinopyroxenes and sulfides, have ratios that are generally elevated slightly above air, whilst bulk samples preserve higher and more variable $^{40}Ar/^{36}Ar$ ratios of ~2000 to 9300 (Fig. 3a). This may indicate siting of ^{40}Ar in grain boundary or fine-matrix material. ^{40}Ar is generally not correlated with K (Fig. 4b), and the $^{40}Ar/K$ ratios measured in most of the RLS samples far exceed those expected for a ~60 Ma intrusion ($^{40}Ar^*/K \approx 6.34 \times 10^{-9}$; Fig. 4b).

448 The excess ^{40}Ar component probably either comes from the mantle source of the
449 Rum intrusion (maximum $^{40}Ar/^{36}Ar$ ~ 44,000; Moreira *et al*., 1998) or from the surrounding
450 crustal rocks. We suggest that the latter is a more likely scenario, given previously
451 documented evidence for crustal contamination in RLS (Palacz 1985; Meyer *et al.* 2009;
452 O'Driscoll *et al.,* 2009), and also a positive correlation between excess ^{40}Ar and I abundance
453 in a subset of the Rum samples (Fig. 3d). Of the three possible K-bearing crustal sources of
454 the excess ^{40}Ar (Archean gneisses, Torridonian sandstones and Mesozoic sediments), it is
455 worth noting that the Torridonian sediments locally contain tourmaline, which is known to
456 host significant ^{40}Ar (several orders of magnitude greater than co-genetic crustal minerals;
457 Saito *et al.,* 1984). Together with the fact that many of the Torridonian sandstones are
458 arkosic (K-rich), they represent at least one potential source for the high ^{40}Ar concentrations
459 observed in the RLS rocks. Alternatively, as noted above, the ^{40}Ar-I relationship seen in the
460 Unit 11-12 rocks (i.e., Fig. 3d) may point to multiple crustal source signatures (^{40}Ar from
461 Lewisian gneisses, I from Mesozoic sediments) being brought together.
462
463 *5.3 Implications for PGE-enrichment and sub-volcanic processing of the halogens*
464 The variations in Rum halogen geochemistry, particularly in the chromitites and associated
465 lithologies (Fig. 5), offer new insights into the mechanisms of precious metal concentration in
466 sub-volcanic systems. The development of PGE-rich chromitite seams in layered intrusions
467 has been attributed to *in situ* reaction of incoming melt with the footwall rocks, i.e., the
468 magma chamber floor, in an essentially metasomatic process (Mathez and Kinzler, 2017). It
469 is important to note in this respect the greater abundances of hydrous phases within Rum
470 chromitite seams, compared to the footwall and hanging wall rocks (Fig. 1c,d). The two key
471 observations from a halogen standpoint for the Rum PGE-rich lithologies are their relatively
472 low Cl and relatively high I abundances. Previous work proposed that the Rum chromitites
473 and anorthosites formed following downward percolation of picritic magma and dissolution of
474 the felspathic footwall (O'Driscoll *et al.* 2010). If the Unit 7 footwall rocks had an I/Cl ratio
475 similar to that of the Unit 10 pegmatoid (RM_16_022) prior to emplacement of the Unit 8

476 magma(s), a reasonable proposition given that there is no chromitite at the base of Unit 11,
477 assimilation of pegmatoidal material could have triggered localised volatile exsolution to
478 produce the hydrous phases in the Unit 7-8 chromitite seam. The relatively low Cl
479 abundances in the chromitites together with localised petrographic evidence for fluid flow
480 probably reflect subsequent volatile loss (Figs. 5, S2d). Furthermore, given the arguments
481 made above for high I concentrations being a consequence of crustal contamination, it would
482 seem that the footwall assimilation process recycled these crustal I signatures to the
483 resultant chromitites. The noble gas isotope data support this conclusion, with well-
484 developed coupled enrichments observed between excess ^{40}Ar and I in the Unit 11
485 anorthosite (Fig. 3d). The Unit 11 anorthosite and Unit 11-12 chromitite plot closely together
486 in I/Cl versus Br/Cl space; suggesting a petrogenetic association between both that is not
487 evident at the Unit 7-8 boundary. This discrepancy could be a consequence of assimilation
488 of compositionally variable footwall.

489 Models for PGE-enrichment in layered intrusions (notably the Stillwater intrusion)
490 appeal to Cl-rich fluids exsolved from the magma to transport and concentrate the PGE into
491 reefs (e.g., Boudreau *et al*. 1986). Such (saline) fluids are known to have high solubilities for
492 the PGE (up to ppm levels; Hanley *et al.* 2005), which could account for the high levels of
493 enrichment in Pt and Pd in the Rum chromitites (e.g., several ppm in the Unit 7-8 chromitite;
494 O'Driscoll *et al.* 2009). However, comparatively little is known about the relationship between
495 the halogens and the base metal sulfides that sequester the PGE in high-temperature
496 magmatic systems. In particular, there are open questions around the ability of crystallising
497 sulfide melt to fractionate the halogens from one another, and whether or not base metal
498 sulfides can host significant halogen concentrations (Mungall and Brenan 2003). Limited
499 experimental evidence suggests halogens preferentially partition into silicate melts during
500 sulfide-silicate melt immiscibility, although sulfide melts are capable of dissolving up to 2000
501 ppm halogens (Mungall and Brenan 2003; Lecumberri-Sanchez and Bodnar 2018). It has
502 been demonstrated that I may be moderately chalcophile (Fuge and Johnson 1984). Whilst
503 Cl may also display chalcophile behaviour, at lower temperatures exsolved halides mix with

aqueous fluids (resulting in high Cl/Br ratio fluids; Mungall and Brenan 2003; Lecumberri-Sanchez and Bodnar 2018); hence, Cl is more easily lost to a fluid phase. Sulfide separates from the Unit 1 troctolite (RM17) and the satellite peridotite plug (RM_16_17) yield higher Br/Cl and I/Cl ratios compared to their respective whole rock values (Fig. 2c, Table 1). Sulfides from the troctolite in particular appear to be enriched in I, by a factor of ~4, compared to their bulk rock counterpart (~24 ppm versus ~6 ppm; Fig. 2b). These troctolites and the satellite peridotites have $\delta^{34}S$ values of -14.8‰ and -18.3‰, respectively, attributed by Hulbert *et al.* (1992) to incorporation of biogenic S from the adjacent Jurassic sediments. It would seem likely that the I enrichment in these rocks also reflects a crustal contamination signature (Fig. S1c). Sulfides are a relatively minor phase in the chromitites (<5 vol.%), so it is unlikely that sulfides alone can account for the entire chromitite I budget. However, the possibility that I may exhibit chalcophile tendencies in high-temperature magmatic systems highlights the need for further experimental work on silicate melt-sulfide melt and sulfide melt-sulfide I partitioning behaviour, to shed light on this relatively poorly constrained part of the I geochemical cycle.

The Rum intrusion was emplaced at a depth of ~2 km and likely underlay a significant volcanic edifice (Emeleus *et al.*, 1996), so the implications of our halogen dataset extend past magma chamber processes and ore genesis, to elucidating the distribution of halogens in sub-volcanic systems prior to and/or during eruption. In particular, I abundances in Rum samples are 12% to two orders of magnitude greater than typical MORB compositions (based on a global range of 1-90 ppb reported by Kendrick *et al.*, 2013), suggesting that crustal contamination might have led to pre-concentration of the halogens in the Rum system before possible injection into the atmosphere on eruption (Aiuppa *et al.,* 2009; Bureau *et al.,* 2000; Pyle and Mather, 2009). Iodine has significantly deleterious effects on atmospheric composition, including tropospheric ozone depletion and the formation of aerosols (e.g., Vogt, 1999). It is worth noting that Rum represents a relatively small (~700 km^3; Emeleus *et al.,* 1996) end-member compared to layered intrusions such as the Bushveld Complex (South Africa), with an estimated magma volume of ~1 × 10^6 km^3

(Cawthorn, 2015). Establishing the abundances and distributions of the heavy halogens in these larger layered intrusions may represent an important avenue for future work, by revealing whether or not the associated magmatism had the potential to introduce significant quantities of I (and Cl, Br) into the atmosphere at punctuated periods in Earth history.

6. Conclusions

In a suite of Rum picrites, cumulates, pegmatoids and chromitites, Cl and Br abundances are present in MORB-relative proportions and correlate well with one another. Their distribution can be accounted for by mineral phases observed in the rocks (e.g., biotite, amphibole and apatite). In the cumulates, these are primary magmatic hydrous phases representing final crystallisation of interstitial liquid in the crystal mush. Iodine behaviour is decoupled from that of Cl and Br; elevated I abundances (and I/Cl ratios relative to MORB) are observed in all samples except for the picrites. The I enrichment points to crustal contamination of the Rum magmas, for which Triassic sedimentary rocks are a likely candidate (maximum 3227 ppm I). Noble gas isotope compositions, particularly $^{40}Ar/^{36}Ar$, also suggest crustal assimilation and in some samples correlate well with I abundance (Fig. 3d). While mass balance calculations suggest that direct solid assimilation fits with previous estimates for the degree of crustal contamination of Rum magmas (based on radiogenic isotopes), this does not explain the fractionation of I from Cl and Br. Instead, addition of a fluid derived by country rock dehydration might better explain the pervasive I enrichment. High I abundances indicate the presence of a crustal component in the PGE-rich chromitites, and together with petrographic evidence for the presence of a fluid phase, suggests reprocessing of pegmatoidal footwall rocks during chromitite petrogenesis. In summary, our study reveals insights into the relative importance of magmatic, crustal contamination and degassing processes in controlling halogen abundances and fractionation in layered intrusions. The importance of aqueous fluids in transporting and redistributing the halogens is emphasised, with implications for their metal-carrying capacity and role in forming magmatic PGE deposits.

Acknowledgements

This manuscript forms a component of A. Parker's PhD thesis undertaken at the University of Manchester, supported by the Natural Environment Research Council grant number NE/L002469/1. Bastian Joachim is thanked for helpful discussions on halogen partitioning. Halogen analyses after pyrohydrolysis were supported by IPGP multidisciplinary program PARI and by Region Île-de-France SESAME Grant no. 12015908. Alan Boudreau and an anonymous reviewer are thanked for their very constructive reviews, as is Tamsin Mather for editorial comments, all of which greatly improved earlier versions of the manuscript.

References

Aiuppa, A., Baker, D.R., and Webster, J.D., (2009). Halogens in volcanic systems. *Chemical Geology*, 263, 1-18. DOI: 10.1016/j.chemgeo.2008.10.005

Allard, P., Burton, M., Sawyer, G., and Bani, P., (2016). Degassing dynamics of basaltic lava lake at a top-ranking volatile emitter: Ambrym volcano, Vanuatu arc. *Earth and Planetary Science Letters,* 448, 69–80. DOI: 10.1016/j.epsl.2016.05.014

Alletti, M., Baker, D.R., Scaillet, B., Aiuppa, A, Moretti, R., and Ottolini, L., (2009). Chlorine partitioning between basaltic melt and H_2O-CO_2 fluids at Mount Etna, *Chemical Geology,* 263,37-50. DOI: 10.1016/j.chemgeo.2009.04.003

Balcone-Boissard, H., Michel, A., and Villemant, B., (2009). Simultaneous determination of fluorine, chlorine, bromine and iodine in six geochemical reference materials using pyrohydrolysis, ion chromatography and inductively coupled plasma-mass spectrometry. *Geostandards and Geoanalytical Research*, 33(4), 477-485. DOI: 10.1111/j.1751-908X.2009.00018.x

584 Bédard, J.H., Sparks, R.S.J., Renner, R., Cheadle, M.J. and Hallworth, M.A. (1988).
585 Peridotite sills and metasomatic gabbros in the Eastern Layered Series of the Rhum
586 complex. *Journal of the Geological Society, London*, 145, 207-224.
587
588 Boudreau, A. E., Mathez, E. A., and McCallum, I. S., (1986). Halogen geochemistry of the
589 Stillwater and Bushveld Complexes: evidence for transport of the platinum-group elements
590 by Cl-rich fluids. *Journal of Petrology,* 27, 967-986. DOI: 10.1093/petrology/27.4.967

591 Brown, G.M., (1956). The Layered Ultrabasic Rocks of Rhum, Inner Hebrides. *Philosophical*
592 *Transactions of the Royal Society of London B: Biological Sciences*, 240(668), 1–54. DOI:
593 10.1098/rstb.1961.0005

594 Bureau, H., Keppler, H., and Métrich, N., (2000) Volcanic degassing of bromine and iodine:
595 experimental fluid/melt partitioning data and applications to stratospheric chemistry. *Earth*
596 *and Planetary Science Letters*, 183, 51-60.

597 Burgess, R., Layzelle, E., Turner, G., and Harris, J.W., (2002). Constraints on the age and
598 halogen composition of mantle fluids in Siberian coated diamonds. *Earth and Planetary*
599 *Science Letters*, 197(3-4), 193–203. DOI: 10.1016/S0012-821X(02)00480-6

600 Cawthorn, R. G., (2015). In: Layered Intrusions (eds. Charlier B., Namur, O., Latypov R. &
601 Tegner, C.) 517–587 (Springer, New York, NY, 2015).
602
603 Déruelle, B., Dreibus, G. and Jambon, A., (1992). Iodine abundances in oceanic basalts:
604 implications for Earth dynamics. *Earth and Planetary Science Letters*, 108(4), pp.217–227.
605 DOI: 10.1016/0012-821X(92)90024-P

606 Edmonds, M., Gerlach, T., and Herd, R.A., (2009) Halogen degassing during ascent and
607 eruption of water-poor basaltic magma. Chemical Geology, 263, 122-130. DOI:
608 10.1016/j.chemgeo.2008.09.022

609 Emeleus, C. H., Cheadle, M.J., Hunter, R. H., Upton, B. G. J., and Wadsworth,W. J. (1996).
610 The Rum Layered Intrusion. *In:* Cawthorn C. G. (Ed.), *Layered Intrusions*, 331–363.

611 Fuge, R., and Johnson, C.C., (1984). Evidence for the chalcophile nature of iodine.
612 *Chemical Geology*, 43, 347-352.

613 Greenwood, R. C., Fallick, A. E., and Donaldson, C. H., (1992). Oxygen isotope evidence for
614 major fluid flow along the contact zone of the Rhum ultrabasic intrusion. *Geological*
615 *Magazine* ,129, 243-246. DOI: 10.1017/S0016756800008311

616 Halter W.E., and Webster J.D, (2004). The magmatic to hydrothermal transition and its
617 bearing on ore-forming systems. *Chemical Geology*, 210(1-4), 1-6. DOI:
618 10.1016/j.chemgeo.2004.06.001

619 Hamilton, M.A., Pearson, D. G, Thompson, R.N., Kelley, S.P., & Emeleus, C.H., (1998).
620 Rapid eruption of Skye lavas inferred from precise U-Pb and Ar-Ar dating of the Rum and
621 Cuillin plutonic complexes. Nature. 394, 260-263. DOI:10.1038/28361

622 Hanley, J. J., Mungall, J. E., Pettke, T., Spooner, E. T. C., & Bray, C. J., (2008). Fluid and
623 halide melt Inclusions of magmatic origin in the ultramafic and lower banded series,
624 Stillwater complex, Montana, USA. Journal of Petrology, 49(6), 1133-1160. DOI:
625 10.1093/petrology/egn020

626 Hanley, J.J., Pettke, T., Mungall, J.E., & Spooner, E.T.C., (2005). The solubility of platinum
627 and gold in NaCl brines at 1.5 kbar, 600 to 800°C: A laser ablation ICP-MS pilot study of
628 synthetic fluid inclusions. Geochimica et Cosmochimica Acta, 69(10), pp.2593–2611. DOI:
629 10.1016/j.gca.2004.11.005

630 Holland, G., and Ballentine, C.J., (2006). Seawater subduction controls the heavy noble gas
631 composition of the mantle. *Nature,* 441, 186–191. DOI: 10.1038/nature04761

632 Holness M.B., (1999). Contact metamorphism and anatexis of Torridonian arkose by minor
633 intrusions of the Rum Igneous Complex, Inner Hebrides, Scotland. *Geological Magazine,*
634 136, 527–542.

635 Hulbert, L.J., Duke, J. M., Ekstrand, O.R., Scoates, R. F. J., Theriault, R.J., Lechminant,
636 M.J., Gunn, A.G. and Grinenko,L.N. (1992). Metallogenic and geochemical evolution of
637 cyclic unit 1, Lower Eastern Layered Series, Rhum. *In*: R.P.Foster (ed.) Mineral Deposit
638 Modelling in Relation to Crustal Reservoirs of the Ore-Forming Elements, London: Institution
639 of Mining and Metallurgy.

640 Kastner, M., Elderfield, H., Martin, J.B., Suess, E., Kvenvolden, K.A., Garrison, R.E., (1990)
641 Diagenesis and interstitial-water chemistry at the Peruvian continental margin-major
642 constituents and strontium isotopes. *In:* Suess, E and von Huene R (*eds*) Proceedings of the
643 ocean drilling program, Scientific results, 112: 413-440.

644 Kendrick, M.A., Kamenetsky, V., Phillips, D., and Honda, M., (2012) Halogen systematics
645 (Cl, Br, I) in Mid-Ocean Ridge Basalts: a Macquarie Island case study. *Geochimica et*
646 *Cosmochimica Acta,* 81, 82–93. DOI: 10.1016/j.gca.2011.12.004

647 Kendrick, M.A., Arculus, R., Burnard, P., and Honda, M. (2013) Quantifying brine
648 assimilation by submarine magmas: Examples from the Galápagos Spreading Centre and
649 Lau Basin. *Geochimica et Cosmochmica Acta*, 123, 150-165.

650 Kendrick, M.A., Jackson, M.G., Kent, A. J.R., Hauri, E.H., Wallace, P.J., and Woodhead, J.,
651 (2014). Contrasting behaviours of CO_2, S, H_2O and halogens (F, Cl, Br, and I) in enriched-
652 mantle melts from Pitcairn and Society seamounts. *Chemical Geology*, 370, 69-81. DOI:
653 10.1016/j.chemgeo.2014.01.019

654 Kendrick, M. A., Hémond, C., Kamenetsky, V.S., Danyushevsky, L., Devey, C.W.,
655 Rodemann, T., Jackson, M.G., and Perfit, M.R., (2017). Seawater cycled throughout Earth's

mantle in partially serpentinized lithosphere. *Nature Geoscience*, 10(3), 222-228. DOI: 10.1038/ngeo2902

Kusebach, C., John, T., Whitehouse, M.J., and Engvik, A.K., (2015) Apatite as a probe for the halogen composition of metamorphic fluids (Bamble Sector, SE Norway). *Contributions to Mineralogy and Petrology*, 170, 34, 20 pp.

Lecumberri-Sanchez P., and Bodnar, R.J., (2018). Halogen Geochemistry of Ore Deposits: Contributions Towards Understanding Sources and Processes. *In:* Harlov, D.E. and Aranovich L., (Eds.) The Role of Halogens in Terrestrial and Extraterrestrial Geochemical Processes. Springer International Publishing, Switzerland.

Lee, J.Y., Marti, K., Severinghaus, J.P., Kawamura, K., Yoo, H.S., Lee, J.B., and Kim, J.S. (2006) A redetermination of the isotopic abundance of atmospheric Ar. Geochimica et Cosmochimca Acta, 70(17), 4507-4512.

Li, Y-H and Schoonmaker, J.E., (2003) Chemical Composition and Mineralogy of Marine Sediments. Treatise on Geochemistry, Executive Editors: Heinrich D. Holland and Karl K. Turekian. pp. 407. Elsevier, p.1-35

Martin, J.M., and Meybeck, M., (1979) Elemental mass balance of material carried by major World rivers. Marine Chemistry, 7(3): 173-206.

Mathez, E.A. and Kinzler, R.J., (2017) Metasomatic chromitite seams in the Bushveld and Rum layered intrusions, *Elements*, 13(6), 397-402.

Matsuda, J., Nagao, K., (1986). Noble-gas abundances in a deep-sea sediment core from eastern equatorial Pacific. *Geochemical Journal*, 20, 71–80. DOI: 10.2343/geochemj.20.71

680 Meyer R., Nicoll G.R., Hertogen J., Troll V.R., Ellam R.M., Emeleus C.H., (2009). Trace
681 element and isotope constraints on crustal anatexis by upwelling mantle melts in the North
682 Atlantic Igneous Province: an example from the Isle of Rum, NW Scotland. *Geological*
683 *Magazine*, 146(3), 382–399. DOI: 10.1017/S0016756809006244

684 Moreira, M., Kunz, J., and Allègre, C. (1998) Rare gas systematics in popping rock: isotopic
685 and elemental compositions in the upper mantle. *Science*, 279, 1178-1181.

686 Mungall, J.E. and Brenan, J.M., (2003). Experimental evidence for the Chalcophile behavior
687 of the halogens. *Canadian Mineralogist*, 41(1), 207–220. DOI: 10.2113/gscanmin.41.1.207

688 Mungall, J.E. and Naldrett, A. J., (2008). Ore Deposits of the Platinum-Group Elements.
689 *Elements*, 4, 253–258. DOI: 10.2113/GSELEMENTS.4.4.253

690 Muramatsu, Y. and Wedepohl, K.H., (1998). The distribution of iodine in the Earth's crust.
691 *Chemical Geology*, 147, 201-216. DOI: 10.1016/S0009-2541(98)00013-8

692 Muramatsu, Y., Doi, T., Tomaru, H., Fehn, U., Takeuchi, R., and Matsumoto, R., (2007)
693 Halogen concentrations in pore waters and sediments of the Nankai Trough, Japan:
694 Implications for the origin of gas hydrates. Applied Geochemistry, 22, 534-556.

695 O'Driscoll, B., Day, James M.D., Daly, S.J., Walker, R.J., and McDonough, W.F., (2009).
696 Rhenium-osmium isotopes and platinum-group elements in the Rum Layered Suite,
697 Scotland: Implications for Cr-spinel seam formation and the composition of the Iceland
698 mantle anomaly. *Earth and Planetary Science Letters*, 286(1-2), 41–51. DOI:
699 10.1016/j.epsl.2009.06.013

700 O'Driscoll, B. Emeleus, C.H., Donaldson, C.H., and Daly, S.J. (2010). Cr-spinel seam
701 petrogenesis in the Rum layered suite, NW Scotland: Cumulate assimilation and in situ
702 crystallization in a deforming crystal mush. *Journal of Petrology*, 51(6), 1171–1201. DOI:
703 10.1093/petrology/egq013

O'Driscoll, B, and VanTongeren, J.A., (2017). Layered Intrusions: From Petrological Paradigms to Precious Metal Repositories. *Elements*, 13(6), 383–389. DOI: 10.2138/gselements.13.6.383

Ozima, M., and Podosek, F.A., (2002). Noble Gas Geochemistry (2nd edition). Cambridge University Press, Cambridge.

Palacz, Z.A., (1985). Sr-Nd-Pb isotopic evidence for crustal contamination in the Rhum intrusion. *Earth and Planetary Science Letters,* 74(1), 35-44. DOI: 10.1016/0012-821X(85)90164-5

Pyle, D.M. & Mather, T.A., (2009). Halogens in igneous processes and their fluxes to the atmosphere and oceans from volcanic activity: A review. *Chemical Geology*, 263(1-4), 110–121.

Reed, M.H., (1997). Hydrothermal alteration and its relationship to ore fluid composition, *In:* Barnes, H.L. (Ed.), Geochemistry of Hydrothermal Ore Deposits, Third Edition. Wiley, New York, pp. 303–366.

Rudnick, R.L., and Gao, S. (2003) Composition of the Continental Crust, *In:* Holland, H.D. and Turekian, K.K. *(Eds) Treatise on Geochemistry*, Elsevier, pp. 659.

Ruzié-Hamilton, L., Clay, P. L., Burgess, R., Joachim, B., Ballentine, C. J., & Turner, G., (2016). Determination of halogen abundances in terrestrial and extraterrestrial samples by the analysis of noble gases produced by neutron irradiation, *Chemical Geology*, 437, 77-87. DOI: 10.1016/j.chemgeo.2016.05.003

Saito, K., Alexander, E.C. Jr., and Dragon, J.C., (1984) Rare gases in cyclosilicates and cogenetic minerals. Journal of Geophysical Research, 89, B9, 7891-79014.

726 Schilling, J.-G., Bergeron, M.B., Evans, R., (1980) Halogens in the Mantle Beneath the North
727 Atlantic. Philosophical Transactions of the Royal Society of London A, 297, 147-178.

728 Schnetger, B., Muramatsu, Y. and Yoshida, S., (1998). Iodine (and Other Halogens) in
729 Twenty-Six Geological Reference Materials by ICP-MS and Ion Chromatography.
730 *Geostandards Newsletter,* 22(2), 181-186. DOI: 10.1111/j.1751-908X.1998.tb00690.x

731 Staudacher, T., and Allègre, C.J., (1988). Recycling of oceanic crust and sediments: the
732 noble gas subduction barrier. *Earth and Planetary Science Letters,* 89, 173–183. DOI:
733 10.1016/0012-821X(88)90170-7

734 Upton, B.G.J., Skovgaard, A.C., McClurg, J., Kirstein, L., Cheadle, M., Emeleus, C.H.,
735 Wadsworth, W.J., & Fallick, A.E., (2002). Picritic magmas and the Rum ultramafic complex,
736 Scotland. *Geological Magazine*, 139, 437–452.

737 Vogt, R., (1999). Iodine compounds in the atmosphere. In: Fabian, P., and Singh, O.N. (eds)
738 Reactive halogen compounds in the atmosphere. The Handbook of Environmental
739 Chemistry (Volume 4 Series Air Pollution), Vol 4E. Springer, Berlin, Heidelberg.

740 von Glasow, R., Bobrowski, N., and Kern, C., (2009). The effects of volcanic eruptions on
741 atmospheric chemistry. *Chemical Geology*. 263, 131–142. DOI:
742 10.1016/j.chemgeo.2008.08.020

743 Webster, J.D., Kinzler, R.J., Mathez, A., (1999). Chloride and water solubility in basalt and
744 andesite melts and implications for magmatic degassing. *Geochimica et Cosmochimica*
745 *Acta,* 63, 729–738. DOI: 10.1016/S0016-7037(99)00043-5

746 **Figure captions**

747 Figure 1. *(a)* Photomicrograph (in cross-polarised light) of a Rum picrite with a groundmass
748 comprising 'sprays' of olivine and plagioclase, suggesting rapid solidification. *(b)*
749 Photomicrograph (in plane-polarised light) of apatite and biotite in a Rum pegmatoid. Ap =
750 apatite, Bt = biotite, Ol = olivine, Plg = plagioclase, Mt = magnetite. *(c)* Backscatter electron
751 micrograph image from approximately 2 mm above the main Unit 7-8 boundary seam (arrow
752 points to location of seam). *(d)* Cl element map (quantified) of the same area as *(c).* Note the
753 presence of elevated Cl concentrations in the groundmass around olivine and Cr-spinel
754 crystals, and in fractures in olivine primocrysts.

755

756 **Figure 2.** Bromine (a) and I (b) normalised to Cl and the Br/Cl and I/Cl (c) ratios for all Rum
757 samples. Mineral separates from picrites, troctolites and pegmatoids are shown as open
758 symbols of the same shape and outline colour as the bulk rock equivalent. MORB data
759 points are small black dots and the reference ratio line is solid black. Data are from Kendrick
760 *et al.* (2012; 2013; 2014). The seawater ratio reference line is dashed and taken from Li and
761 Schoonmaker (2003). Marine sediments and pore fluids (pore fluids describe the typically Br-
762 and I-rich fluid phase recovered from sedimentary cores; n =134, grey crosses) data are
763 from Muramatsu *et al.* (2007), Martin *et al.* (1993) and Kastner *et al.* (1990). Average
764 continental crust is represented as a brown-outlined star and is from Rudnick and Gao
765 (2003). Subcontinental lithospheric mantle (SCLM) from Burgess *et al.* (2002) is represented
766 by red star symbols. In (c), a global marine shale average composition is depicted as a
767 black-outline triangle (Li and Schoonmaker, 2003).

768

769 **Figure 3.** *(a)* Age-corrected $^{40}Ar/^{36}Ar$ ratio as a function of the molar $Cl/^{36}Ar$ (x 10^{-6}) in the
770 RLS rocks by sample type. Mineral separates from picrites, troctolites and pegmatoids are
771 shown as open symbol of the same shape and outline colour as the bulk rock equivalent.
772 Two trends are observed for the bulk rock and mineral separates (inset) with different $^{40}Ar/Cl$
773 ratios. The $^{40}Ar/^{36}Ar$ ratio in air ($^{40}Ar/^{36}Ar_{air}$ = 298.56; Lee *et al.,* 2006) is shown by the dashed

774 black line. The potential influence of crustal input to the elevated $^{40}Ar/^{36}Ar$ ratio is shown
775 schematically. *(b)* Molar $^{40}Ar/Cl$ as a function of the molar K/Cl ratio by sample type. The lack
776 of correlation indicates the ^{40}Ar is decoupled from the K-content and therefore not the result
777 of in *situ* K-decay (excess Ar). The $^{40}Ar/K$ ratio for the 60 Ma is ~ 6.34×10^{-9}, which is
778 essentially at the origin in this plot. . The mineral separates (inset) show a distinct trend
779 compared to the bulk rock samples. *(c)* The molar $^{40}Ar/K$ ($\times 10^{-5}$) ratio as a function of the
780 molar I/K ratio ($\times 10^{5}$) in the RLS. Mineral separates from the pegmatoids show a high I/K
781 ratio weakly correlated with their low $^{40}Ar/K$ ratio - see also inset and (d). *(d)* Excess ^{40}Ar
782 (mol/g) as a function of I (mol/g) concentration in the Unit 11-12 peridotite, anorthosite and
783 chromitites. The long dash line (R^2=0.99) is a linear fit to the B2 chromitite data (black
784 squares) and one B2 anorthosite point (blue squares). The short dash line (R^2=0.99) is a
785 linear fit to the B2 peridotite data (green squares) and data for three B2 anorthosite samples.
786
787
788 **Figure 4.** $^{130}Xe/^{36}Ar$ versus $^{84}Kr/^{36}Ar$ isotope plot of all RLS rocks. Mineral separates from
789 picrites, troctolites and pegmatoids are shown as open symbol of the same shape and
790 outline colour as the bulk rock equivalent. Reference values, including, MORB (orange
791 outline stars) include Bravo Dome and 'popping rock', seawater (grey outline star) and air
792 (blue outline star); data from Moreira *et al.* (1998), Holland and Ballentine (2006) and Ozima
793 and Podosek (2002). The marine sediments range (grey field) is a reference range from
794 Ozima and Podosek (2002).
795
796 **Figure 5.** Halogen data (Cl data in ppm and Br and I data in ppb) as a function of the
797 stratigraphic column of units 7 to 14 of the Eastern Layered Intrusion of Rum, including
798 schematic diagrams of unit boundary textural relationships where the PGE-rich chromitites
799 occur (redrawn after O'Driscoll *et al.* 2009). Halogens show the full range (e.g., all replicate
800 analyses; Table S2) of data. PGE data of O'Driscoll *et al.* (2009) are included for
801 comparison.

Figure 1

Click here to download high resolution image

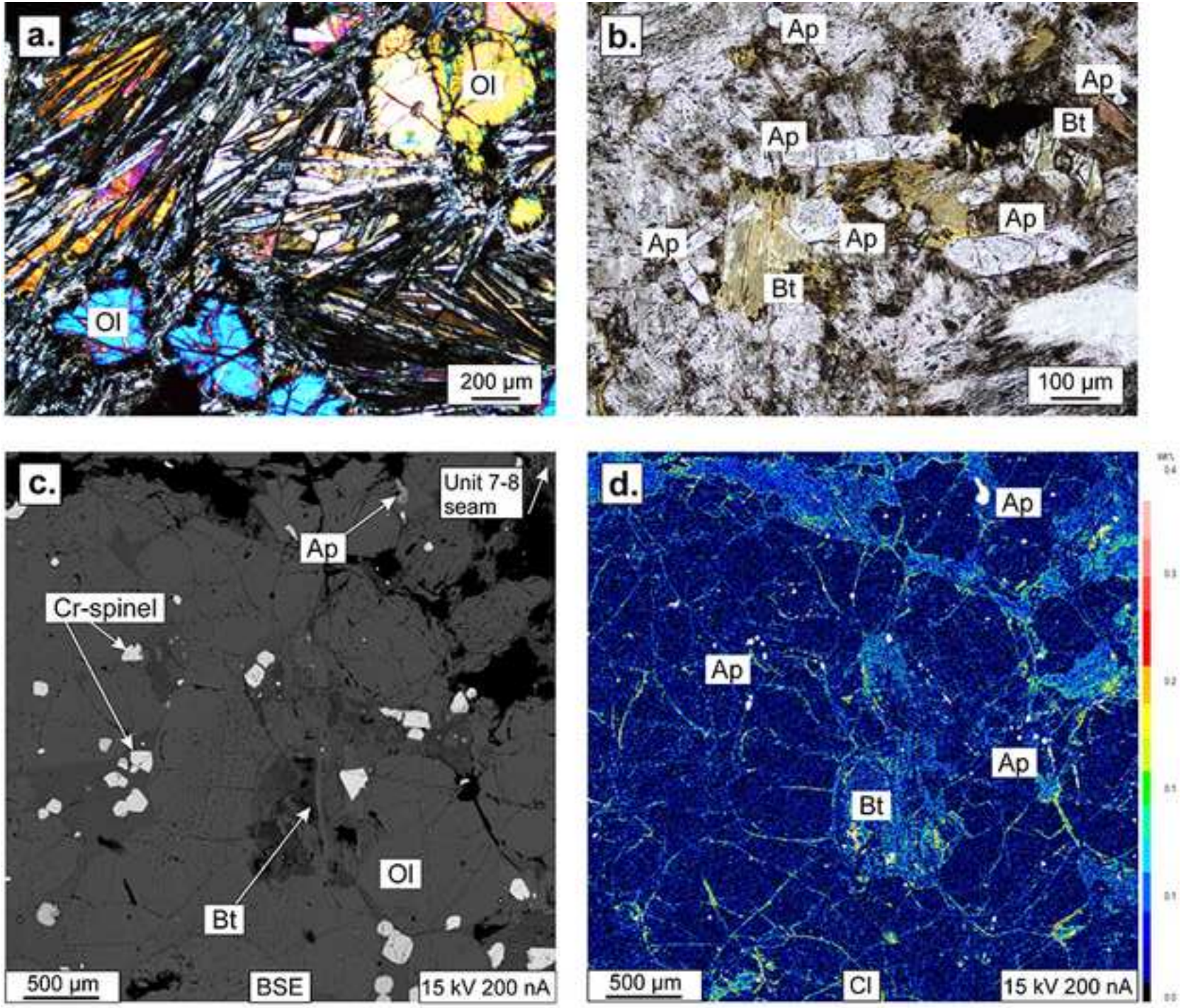

Figure 2

Click here to download high resolution image

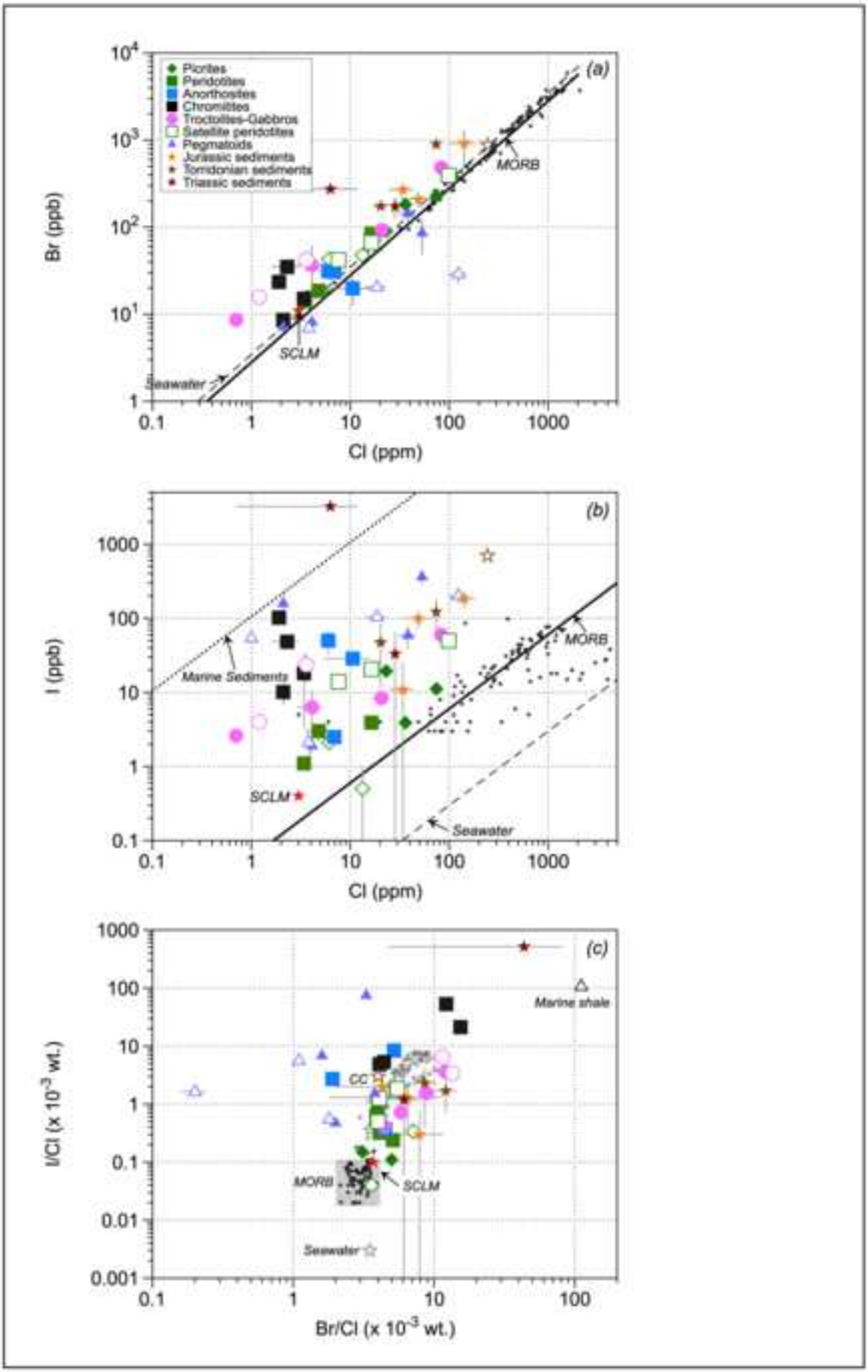

Figure 3

Click here to download high resolution image

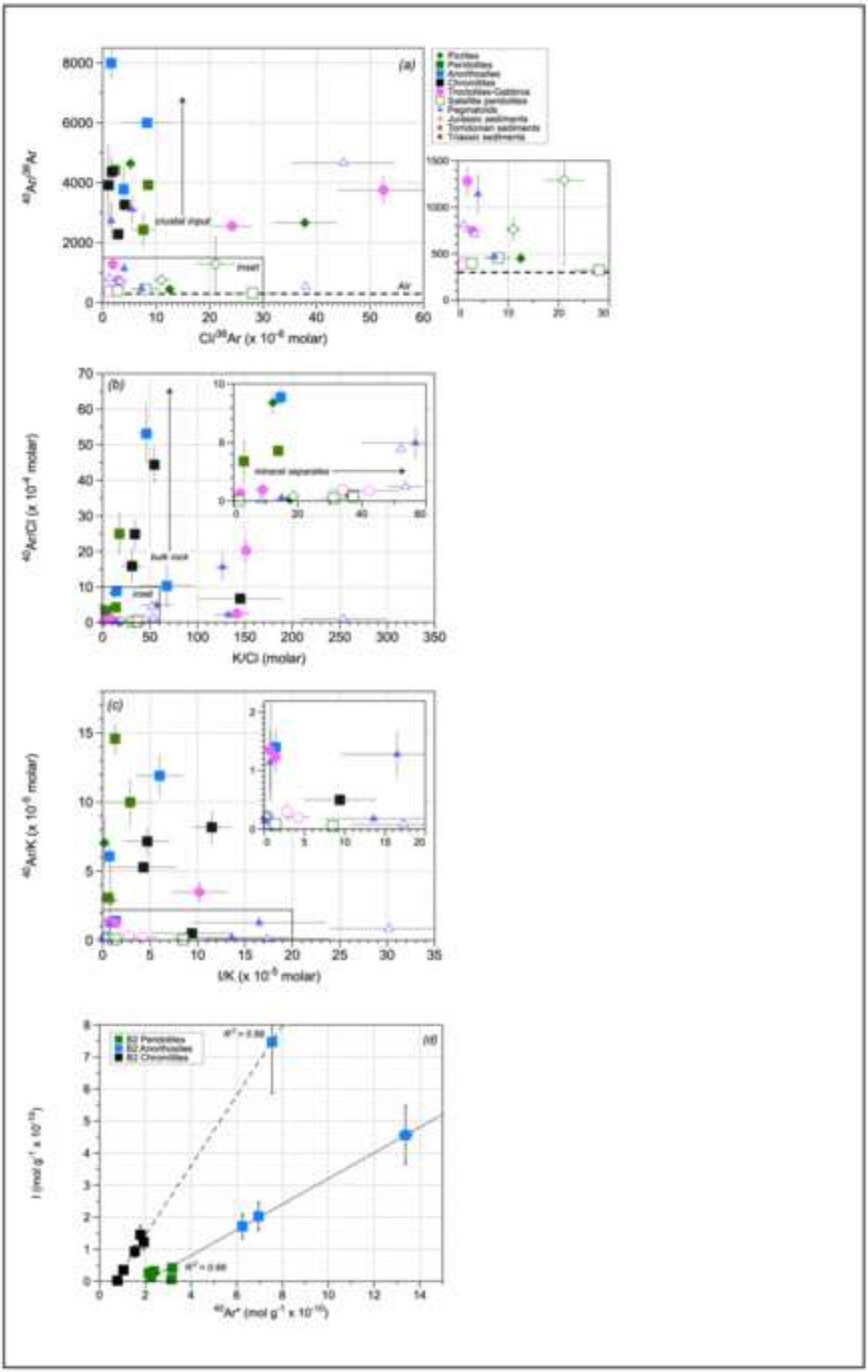

Figure 4

Click here to download high resolution image

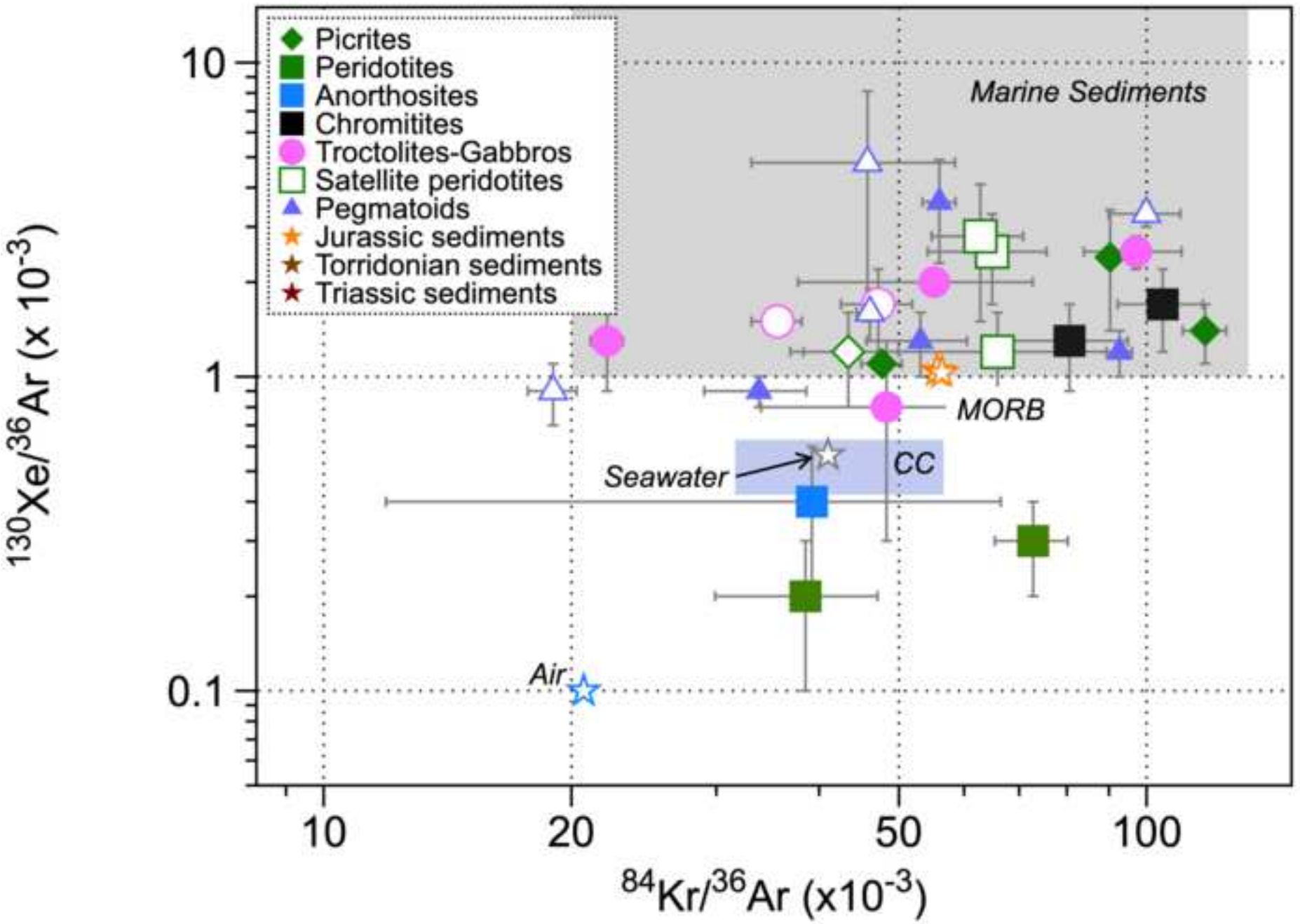

Figure 5

Click here to download high resolution image

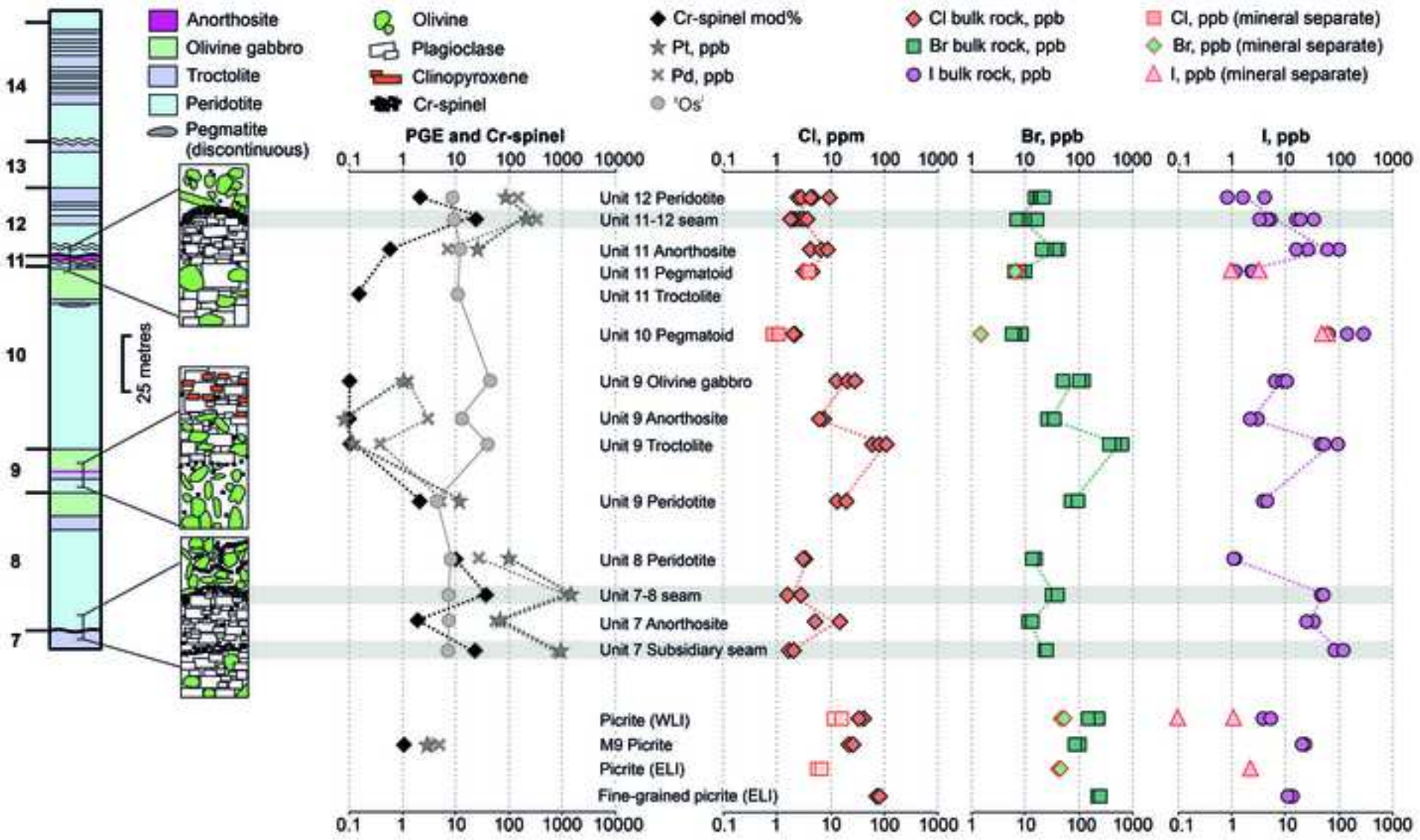

Table 1

Click here to download Table: Table 1-revised.xlsx

Table 1. Sample lithology/provenance details and K and halogen abundances/ratios. Data are averages and the uncertainties are 1 sigma SEM

Sample ID	Sample lithology/provenance*	Sample type	K (ppm)	Cl (ppm)	Br (ppb)	I (ppb)	K/Cl (wt.)	Br/Cl (wt. x10^{-3})	I/Cl (wt. x10^{-3})
Picrites									
M9 Picrite	M9 Picrite, WLI	Bulk	451 ± 69	23.1 ± 2.0	89.9 ± 5.4	19.4 ± 0.5	19.4 ± 1.3	3.89 ± 0.06	0.84 ± 0.02
RM_16_010 Olivine	Picrite (olivine), ELI	Separate	125 ± 19	6.1 ± 0.5	43 ± 0.2	2.1 ± 0.1	20.5 ± 1.4	7.1 ± 0.08	0.34 ± 0.01
RM_16_011	Picrite (fine grained), ELI	Bulk	2908 ± 94	74.5 ± 4.7	229 ± 14	11.2 ± 1.2	39.1 ± 1.2	3.07 ± 0.04	0.15 ± 0.01
RM4 (RM_16_012)	Picrite, WLI	Bulk	484 ± 19	36.1 ± 3.8	181.6 ± 35.4	3.9 ± 0.6	13.6 ± 2	5.03 ± 0.16	0.11 ± 0.01
RM_16_012 Olivine	Picrite (olivine), WLI	Separate	17 ± 8	13.3 ± 2.2	47.8 ± 5	0.5 ± 0.5	1.2 ± 0.4	3.59 ± 0.12	0.04 ± 0.01
Rum intrusion rocks									
B2 Peridotite	Unit 12 peridotite, ELI	Bulk	71 ± 6	4.8 ± 1.3	18.6 ± 1.2	3.0 ± 0.8	19.5 ± 5	3.9 ± 0.16	0.63 ± 0.07
B2 Anorthosite	Unit 11 anorthosite, ELI	Bulk	283 ± 39	6 ± 1.1	31.1 ± 4.7	50.1 ± 17	50.8 ± 9.1	5.2 ± 0.18	8.38 ± 0.83
B2 Chromite	Unit 11-12 Chromitite, ELI	Bulk	77 ± 3	2.1 ± 0.2	8.6 ± 0.5	10.1 ± 3.4	37.5 ± 2.5	4.14 ± 0.06	4.84 ± 0.49
RM11 Chromitite	Unit 11-12 Chromitite, ELI	Bulk	120 ± 54	3.4 ± 0.3	15.1 ± 1.7	18.1 ± 14.9	34.2 ± 12.9	4.45 ± 0.09	5.31 ± 0.10
U9 Troctolite	Unit 9 troctolite, ELI	Bulk	179 ± 6	83.1 ± 14.3	484.5 ± 77.8	60 ± 14.2	2.3 ± 0.5	5.83 ± 0.19	0.72 ± 0.07
U9 Olivine Gabbro	Unit 9 gabbro ELI	Bulk	181 ± 21	20.7 ± 4.5	92.1 ± 21.6	8.4 ± 1.2	10 ± 2.9	4.44 ± 0.18	0.41 ± 0.03
U9 Peridotite	Unit 9 Peridotite, ELI	Bulk	53 ± 13	16.4 ± 3	84.2 ± 14.2	3.9 ± 0.4	3.5 ± 1.4	5.14 ± 0.17	0.24 ± 0.01
U9 Anorthosite	Unit 9 anorthosite, ELI	Bulk	111 ± 4	6.9 ± 0.6	30.6 ± 5.1	2.5 ± 0.4	16.2 ± 0.9	4.46 ± 0.09	0.37 ± 0.02
U7-8 Peridotite	Unit 8 peridotite, ELI	Bulk	52 ± 1	3.4 ± 0.1	14 ± 0.6	1.1 ± 0.1	15.4 ± 0.2	4.15 ± 0.03	0.32 ± 0.01
C8 Chromite-Peridotite	Unit 8 chromitite-peridotite boundary, ELI	Bulk	319 ± 126	1.9 ± 0.2	23.5 ± 0.5	102.1 ± 19.1	160 ± 49	12.16 ± 0.15	52.85 ± 3.23
RM_16_008	Unit 7-8 chromitite, ELI	Bulk	135 ± 36	2.3 ± 0.7	35 ± 4	48.2 ± 2.2	60.1 ± 1.7	15.39 ± 0.58	21.19 ± 1.86
C8 Anorthosite	Unit 7 anorthosite, ELI	Bulk	624 ± 48	10.6 ± 5.2	19.8 ± 7.3	28.7 ± 4.4	74.7 ± 32	1.87 ± 0.14	2.71 ± 0.47
RM17 Troctolite	Unit 1 troctolite, ELI	Bulk	665 ± 245	4.1 ± 1.2	36.5 ± 25	6.3 ± 4.4	156.1 ± 15.7	8.8 ± 1.14	1.53 ± 0.28
RM17 Sulfide	Unit 1 troctolite (sulfide), ELI	Separate	164 ± 8	3.6 ± 0.6	42 ± 10.8	23.5 ± 9.7	46.7 ± 10	11.51 ± 0.42	6.44 ± 0.77
RM7 Olivine gabbro	Gabbro (cpx-rich), CI	Bulk	119 ± 8	0.7 ± 0.02	8.6 ± 1.6	2.6 ± 0.6	166.8 ± 5.9	12.1 ± 0.24	3.58 ± 0.24
RM7 Cpx	Gabbro (cpx-rich), CI	Separate	44 ± 6	1.2 ± 0.1	15.7 ± 0.8	4.0 ± 0.4	37.6 ± 5.1	13.52 ± 0.09	3.41 ± 0.10
Satellite intrusion rocks									
RM_16_013	Satellite peridotite plug, West Sgaorishal	Bulk	186 ± 20	98.7 ± 11.9	393.8 ± 61.7	49.7 ± 0.3	1.9 ± 0.4	3.99 ± 0.1	0.50 ± 0.02
RM_16_017	Satellite peridotite plug, West Sgaorishal	Bulk	568 ± 112	16.4 ± 1.2	66.7 ± 1.5	20.5 ± 2.0	34.4 ± 4.3	4.08 ± 0.04	1.25 ± 0.04
RM_16_017 Sulfide	Satellite peridotite plug (sulfide), West Sgaorishal	Separate	314 ± 11	7.6 ± 0.2	42 ± 2.6	13.9 ± 2.8	41.2 ± 2.6	5.5 ± 0.05	1.83 ± 0.10
Pegmatoids									
RM_16_022 A	Unit 10 pegmatoid, ELI	Bulk	295 ± 12	2.1 ± 0.05	7.1 ± 0.8	158 ± 62.2	139.4 ± 8.7	3.32 ± 0.05	74.31 ± 8.27
RM_16_022 Amphibole	Unit 10 pegmatoid (amphibole), ELI	Separate	56 ± 8	1.0 ± 0.1	nd	53.8 ± 6.1	57.5 ± 0.6	nd	55.15 ± 2.78
RM_16_024	Unit 11 Pegmatoid, ELI	Bulk	586 ± 8	4.1 ± 0.5	8.1 ± 1.0	1.9 ± 0.4	146.6 ± 16.3	1.98 ± 0.06	0.47 ± 0.03
RM_16_024 Amphibole	Unit 11 Pegmatoid (amphibole), ELI	Separate	226 ± 32	3.8 ± 0.2	6.9 ± 0.2	2.1 ± 1.1	59 ± 6	1.82 ± 0.01	0.55 ± 0.08
RM3 Pegmatoid	Pegmatoid, WLI	Bulk	2569 ± 907	38.3 ± 7.8	143.7 ± 30	58.7 ± 20.6	62.5 ± 18.7	3.75 ± 0.07	1.53 ± 0.18
RM_16_021 A	Pegmatoid, CI	Bulk	861 ± 94	53.2 ± 4.5	85.8 ± 37.4	362.7 ± 81.9	16.6 ± 2.3	1.61 ± 0.08	6.82 ± 0.47
RM_16_021 Amphibole	Pegmatoid (amphibole), CI	Separate	187 ± 70	18.6 ± 4.3	20.4 ± 1.5	103.7 ± 13	9.7 ± 1.5	1.1 ± 0.04	5.57 ± 0.44
RM_16_021 Biotite	Pegmatoid (biotite), CI	Separate	34739 ± 6184	124 ± 26.3	28.9 ± 6.3	200.7 ± 40.1	280 ± 49.9	0.23 ± 0.04	1.62 ± 0.13

**ELI, WLI and CI are Eastern Layered Intrusion, Western Layered Intrusion and Central Intrusion, respectively*